Received: 4 January 2019 | Revised: 17 June 2019 | Accepted: 25 June 2019

DOI: 10.1002/ajpa.23899

RESEARCH ARTICLE

American Journal of PHYSICAL ANTHROPOLOGY WILEY

Morphological integration affects the evolution of midline cranial base, lateral basicranium, and face across primates

Dimitri Neaux[1,2,3] | Stephen Wroe[2] | Justin A. Ledogar[4] | Sarah Heins Ledogar[5] | Gabriele Sansalone[2,6,7]

[1]Archéozoologie, Archéobotanique: Sociétés, Pratiques et Environnements (AASPE), UMR 7209, Muséum national d'Histoire naturelle-CNRS, Paris, France

[2]Function, Evolution & Anatomy Research Lab, School of Environmental and Rural Science, University of New England, Armidale, New South Wales, Australia

[3]Laboratoire Paléontologie Evolution Paléoécosystèmes Paléoprimatologie (PALEVOPRIM), UMR 7262, Université de Poitiers-CNRS, Poitiers, France

[4]Department of Evolutionary Anthropology, Duke University, Durham, North Carolina

[5]Department of Archaeology & Palaeoanthropology, School of Humanities, University of New England, Armidale, New South Wales, Australia

[6]Department of Sciences, Roma Tre University, Rome, Italy

[7]Center for Evolutionary Ecology, Rome, Italy

Correspondence
Dimitri Neaux, CNRS-Muséum national d'Histoire naturelle, UMR 7209, Archéozoologie, Archéobotanique: Sociétés, Pratiques et Environnements, CP 56, 55 rue Buffon, 75005 Paris, France.
Email: dimitrineaux@gmail.com

Funding information
Australian Research Council Discovery grant, Grant/Award Number: DP140102659

Abstract

Objectives: The basicranium and face are two integrated bony structures displaying great morphological diversity across primates. Previous studies in hominids determined that the basicranium is composed of two independent modules: the midline basicranium, mostly influenced by brain size, and the lateral basicranium, predominantly associated with facial shape. To better assess how morphological integration impacts the evolution of primate cranial shape diversity, we test to determine whether the relationships found in hominids are retained across the order.

Materials and methods: Three-dimensional landmarks (29) were placed on 143 computed tomography scans of six major clades of extant primate crania. We assessed the covariation between midline basicranium, lateral basicranium, face, and endocranial volume using phylogenetically informed partial least squares analyses and phylogenetic generalized least squares models.

Results: We found significant integration between lateral basicranium and face and between midline basicranium and face. We also described a significant correlation between midline basicranium and endocranial volume but not between lateral basicranium and endocranial volume.

Discussion: Our findings demonstrate a significant and pervasive integration in the craniofacial structures across primates, differing from previous results in hominids. The uniqueness of module organization in hominids may explain this distinction. We found that endocranial volume is significantly integrated to the midline basicranium but not to the lateral basicranium. This finding underlines the significant effect of brain size on the shape of the midline structures of the cranial base in primates. With the covariations linking the studied features defined here, we suggest that future studies should focus on determining the causal links between them.

KEYWORDS
endocranium, geometric morphometrics, modularity, skull

1 | INTRODUCTION

There is considerable cranial morphological diversity across the nearly 500 species, and more than 70 genera, of extant primates (Mittermeier, Rylands, & Wilson, 2013; Rylands & Mittermeier, 2014). Much of this variation is located in the basicranium and in the facial skeleton (Bennett & Goswami, 2012; Fleagle, Gilbert, & Baden, 2010, 2016). Currently, identifying the processes that have driven this morphological

diversity is a critical question in the field of biological anthropology (Neaux et al., 2018; Profico et al., 2017; Ritzman et al., 2017; Schroeder & von Cramon-Taubadel, 2017). Previous studies suggest that the face and the basicranium evolved in a coordinated fashion, evincing a key role for morphological integration in shaping the phenotypic diversity of the primate cranium (Bastir & Rosas, 2006, 2016; Marroig & Cheverud, 2001; Marroig, De Vivo, & Cheverud, 2004; Neaux, 2017; Neaux et al., 2018; Singh, Harvati, Hublin, & Klingenberg, 2012; Strait, 2001). It has been proposed that morphological integration between biological structures has been a major influence on the evolution of phenotypic variation (Klingenberg, 2005; Schlosser & Wagner, 2004; Wagner & Altenberg, 1996). A high degree of covariation between structures (i.e., strong integration) channels morphological variation along specific trajectories of phenotypic space, corresponding to paths of least resistance (Goswami & Polly, 2014; Klingenberg, 2010; Wagner, Pavlicev, & Cheverud, 2007). This coinheritance of character complexes has been described as the consequence of shared genetic processes, developmental pathways, functional selective pressures, and/or phylogenetic constraints (Lieberman, 2011; Marcucio, Young, Hu, & Hallgrimsson, 2011; Martínez-Abadías, Esparza, Sjøvold, & Hallgrímsson, 2016; Parsons et al., 2011; Parsons, Downey, Jirik, Hallgrimsson, & Jamniczky, 2015). Therefore, the study of morphological integration gives access to a unique comprehensive system linking genetics, development, functions, and phylogeny into unified, realistic, and informed models of evolution (Goswami & Polly, 2014).

Focusing on modern humans, Bastir and Rosas (2005, 2006, 2009) made a major advance in the comprehension of cranial integration, determining that the basicranium is composed of two modules, that is, morphological structures with a stronger integration within than between them (Klingenberg, 2008). The first module is the midline basicranium (MB), formed by the cribriform plate, the planum sphenoidale, the sella turcica, and the clivus. The second is the lateral basicranium (LB), composed of the anterior cranial fossae, the middle cranial fossae, and the posterior cranial fossae. Bastir and Rosas (2005, 2006, 2009) found significant integration between LB and face, but not between MB and face. They suggested that the duration of common developmental timing acts on the degree of craniofacial integration. Indeed in modern humans MB matures first (7–8 years old), followed by LB (11–12 years old), and face (15–16 years old; Bastir, Rosas, & O'Higgins, 2006; Lieberman & McCarthy, 1999). Previous two-dimensional studies including all major clades of primates (i.e., hominoids, cercopithecines, colobines, platyrrhines, lemuriformes, and lorisiformes) showed a strong correlation between MB shape and endocranial volume (ECV; Bastir et al., 2010; Lieberman, Ross, & Ravosa, 2000; Ross & Ravosa, 1993; Strait & Ross, 1999). These results suggest that variation in MB shape is mainly a structural response, needed to generate enough space in the braincase for an enlarged brain.

The findings of Bastir and Rosas (2005, 2006, 2009) were based on analyses of modern humans. Two more recent studies have shown that the described integration (i.e., facial shape is significantly related to LB but not to MB and ECV is significantly related MB but not to LB) is likely to occur also among other primates (Aristide et al., 2015; Neaux, Guy, Gilissen, Coudyzer, & Ducrocq, 2013). First, Neaux et al. (2013) found integration similar to those of modern humans (i.e., nonsignificant between MB and face but significant between LB and face) in the common chimpanzee (*Pan troglodytes*), despite the extended postnatal growth trajectory of MB in this taxa (Lieberman & McCarthy, 1999). More recently still, Aristide et al. (2015) described a significant correlation between MB and encephalization, but not between LB and encephalization in platyrrhines.

Bastir and Rosas (2005, 2006, 2009) highlighted the decisive role of morphological integration in shaping the human basicranium and face. Yet, a comprehensive study of the impact of the covariation between these structures across primates is still lacking. By including representatives of each major clade of primates (i.e., hominoids, cercopithecines, colobines, platyrrhines, lemuriformes, and lorisiformes), the present study allows a more thorough evaluation of the impact of phenotypic integration on cranial variation among primates. Here, we assess how morphological integration affects the relationship between basicranial (MB and LB) and facial evolutionary pathways. We employ 3D geometric morphometrics (GMM) and phylogenetic comparative methods to determine whether the type of integration described in modern humans (Bastir & Rosas, 2005, 2006, 2009) exists across primates. We test the hypotheses that facial shape is significantly related to LB but not to MB (hypothesis 1). Furthermore, we evaluate whether MB shape is a structural response for an enlarged brain (Lieberman et al., 2000; Ross & Ravosa, 1993; Strait & Ross, 1999) by testing if ECV is significantly related to MB but not to LB (hypothesis 2). We predict that facial shape is significantly related to LB but not to MB (hypothesis 1) and that ECV is significantly related to MB but not to LB (hypothesis 2).

2 | MATERIALS AND METHODS

2.1 | Sample

The sample consisted of 143 crania of extant primates belonging to 55 different species (Table 1, Appendix S1), constituting a representative sample of the diversity of the order, that is, ~75% of the recognized extant genera (Groves, 2001). Following Neaux et al. (2018), we identified six major clades of primates: hominoids, cercopithecines, colobines, platyrrhines, lemuriformes, and lorisiformes (Table 1). One to three individuals represented each species, depending of the availability of the specimens. The sample included males and females for each species wherever possible. Our study focused on integration at the interspecific level and was designed to examine shared patterns of morphological covariation between different primate clades. For this reason, we chose to include a large number of species rather than a large number of specimens for each species. Small samples per species can be considered as a limitation to achieving adequate estimates of between-species variation. Yet, when shape differences among samples are large and increasing the number of samples is more important than sample size within each sample, a few individual per sample may suffice (Cardini, Seetah, & Barker, 2015). Computed tomography (CT) scans were obtained from MorphoSource (Aguilar, Boyer, Carney, et al., 2017; Aguilar, Boyer, Heritage, et al., 2017; Allen & Schaeffer, 2017; Copes, Kaufman, & Lee, 2017) and National Museum of Natural

TABLE 1 Species included in the study, taxonomic groups, and number of specimens (*n*), males (m), females (f), and not determined individuals (nd)

Species	Taxonomic group	*n* (m,f,nd)
Bunopithecus hoolock	Hominoidea	2 (0,2,0)
Gorilla beringei	Hominoidea	3 (1,2,0)
Homo sapiens	Hominoidea	3 (2,1,0)
Hylobates lar	Hominoidea	3 (1,2,0)
Nomascus leucogenys	Hominoidea	3 (0,3,0)
Pan troglodytes	Hominoidea	3 (1,2,0)
Pongo abelii	Hominoidea	3 (1,2,0)
Symphalangus syndactylus	Hominoidea	3 (2,1,0)
TOTAL	Hominoidea	23 (8,14,0)
Allenopithecus nigroviridis	Cercopithecinae	2 (0,1,1)
Cercocebus torquatus	Cercopithecinae	2 (1,1,0)
Cercopithecus mitis	Cercopithecinae	3 (1,2,0)
Chlorocebus sabaeus	Cercopithecinae	2 (1,1,0)
Erythrocebus patas	Cercopithecinae	3 (1,1,1)
Lophocebus albigena	Cercopithecinae	3 (1,2,0)
Macaca fascicularis	Cercopithecinae	3 (0,2,1)
Mandrillus leucophaeus	Cercopithecinae	3 (3,0,0)
Miopithecus talapoin	Cercopithecinae	2 (1,1,0)
Papio anubis	Cercopithecinae	3 (2,1,0)
Theropithecus gelada	Cercopithecinae	2 (1,1,0)
TOTAL	Cercopithecinae	28 (12,13,3)
Nasalis larvatus	Colobinae	3 (2,1,0)
Piliocolobus badius	Colobinae	3 (1,2,0)
Presbytis rubicunda	Colobinae	3 (1,1,1)
Pygathrix nemaeus	Colobinae	2 (1,1,0)
Rhinopithecus roxellana	Colobinae	2 (2,0,0)
Semnopithecus priam	Colobinae	3 (1,2,0)
Trachypithecus cristatus	Colobinae	3 (1,2,0)
TOTAL	Colobinae	19 (9,9,1)
Alouatta caraya	Platyrrhini	3 (1,1,1)
Aotus trivirgatus	Platyrrhini	3 (1,1,1)
Ateles geoffroyi	Platyrrhini	3 (1,1,1)
Cacajao calvus	Platyrrhini	3 (1,1,1)
Callicebus moloch	Platyrrhini	3 (3,0,0)
Callithrix argentata	Platyrrhini	3 (2,1,0)
Cebus capucinus	Platyrrhini	3 (0,3,0)
Chiropotes satanas	Platyrrhini	3 (2,1,0)
Lagothrix lagotricha	Platyrrhini	3 (1,1,1)
Leontopithecus rosalia	Platyrrhini	3 (0,3,0)
Pithecia monachus	Platyrrhini	2 (1,0,1)
Saimiri sciureus	Platyrrhini	3 (2,1,0)
TOTAL	Platyrrhini	35 (15,14,6)
Avahi laniger	Lemuriformes	1 (1,0,0)
Daubentonia madagascariensis	Lemuriformes	2 (1,0,1)
Eulemur fulvus	Lemuriformes	2 (0,2,0)
Hapalemur griseus	Lemuriformes	2 (1,1,0)
Lemur catta	Lemuriformes	3 (2,0,1)
Lepilemur mustelinus	Lemuriformes	1 (0,0,1)
Microcebus murinus	Lemuriformes	3 (2,0,1)
Mirza coquereli	Lemuriformes	1 (0,0,1)
Propithecus verreauxi	Lemuriformes	3 (1,0,2)
Varecia variegata	Lemuriformes	2 (0,0,2)
TOTAL	Lemuriformes	20 (8,3,9)
Arctocebus aureus	Lorisiformes	3 (2,1,0)
Euoticus elegantulus	Lorisiformes	3 (2,1,0)
Galago senegalensis	Lorisiformes	3 (2,1,0)
Loris lydekkerianus	Lorisiformes	2 (1,1,0)
Nycticebus coucang	Lorisiformes	3 (1,0,2)
Otolemur crassicaudatus	Lorisiformes	1 (0,0,1)
Perodicticus potto	Lorisiformes	3 (1,1,1)
TOTAL	Lorisiformes	18 (9,5,4)

History (http://humanorigins.si.edu/evidence/3d-collection/primate) digital repositories. The original skeletal materials belong to the collections of the Museum of Comparative Zoology at Harvard University (Cambridge), the National Museum of Natural History (Washington), the Natural History Museum (London, UK), and the Duke Lemur Center (Durham). All specimens were adults, that is, third molars were fully erupted. We created three-dimensional (3D) virtual representations in PLY file format from CT scans with voxel size and slice thickness ranging from 0.3 mm to 1 mm depending of their digital repositories. We subsequently removed the upper part of the calvaria with Geomagic v.2014 software to access internal basicranial structures (Figure 1).

2.2 | Data acquisition

We used 29 symmetrized 3D landmark coordinates collected bilaterally to describe MB, LB, and face (Figure 1, Table 2). MB and LB are each represented by the same number of landmarks (7) so as to allow a comparable measure of integration (Mitteroecker & Bookstein, 2007). One of us (D.N.) digitized landmarks on the 3D polygonal surfaces with IDAV Landmark v3.0 software (Wiley et al., 2005). To test for reproducibility, we computed a one-way multivariate analysis of variance (MANOVA) on the landmark coordinates of three *Hylobates lar* specimens resampled three times on three different days by D.N. Measurement errors show no significant differences between the repeated samples (Wilk's $\lambda = 0.99$, $F[2,84] = 0.05$, $p = .96$) confirming that the measurement errors were smaller than the among-specimen variance. We measured the ECV of each specimen from virtual endocasts generated from the CT data (Appendix S2). The phylogenetic tree used in the following analyses is a time-calibrated consensus tree based on a Bayesian estimate

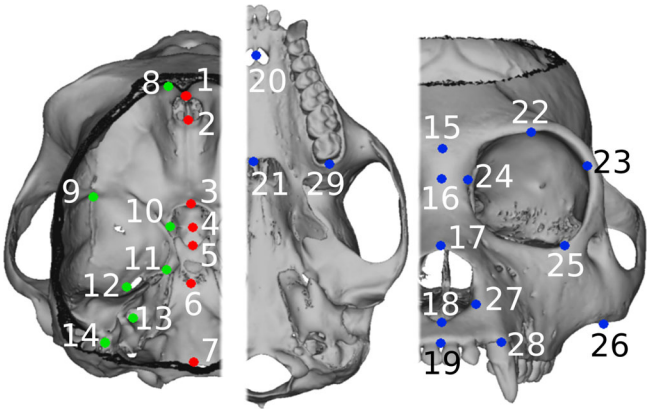

FIGURE 1 *Alouatta caraya* cranium showing the midline basicranial (1–7; red), lateral basicranial (8–14; green), and facial (15–29; blue) landmarks used in the study in superior, inferior, and frontal views

obtained from the 10kTrees Project v.3 for the 55 species in our dataset (Arnold, Matthews, & Nunn, 2010).

2.3 | Statistics

We performed all analyses in the R statistical environment (R Core Team, 2017). We used a generalized Procrustes analysis (Rohlf & Slice, 1990), implemented in the procSym() function from the package "Morpho" (Schlager & Jefferis, 2016) to rotate, translate, and scale landmark configurations to unit centroid size (CS), the square root of the sum of squared distances of the landmarks from their centroid (Bookstein, 1991). The procSym() function removes the asymmetrical component following Klingenberg, Barluenga, and Meyer (2002). For each landmark configuration, a reflected and relabeled duplicate is added to the dataset, a simultaneous Procrustes fit is computed for all the configurations, and subsequent analyses are based on the averaged Procrustes coordinates of each specimen and its mirror image. This provides a multivariate space of the appropriate dimensionality to study shape variations. We performed a multivariate regression of shape on the logarithm of centroid size (shape and logarithm of centroid size were both averaged by species) to test the relationship between size (independent variable) and shape (dependent variable).

Allometry is suggested to play an important role in shaping the patterns of morphological integration at both interclade and intraclade level (Klingenberg & Marugán-Lobón, 2013). To study interclade shape differences, the intraclade variation due to size was removed by performing separate per-clade (hominoids, cercopithecines, colobines, platyrrhines, lemuriformes, and lorisiformes; Table 1) multivariate regressions between shape and size. Then, for each clade, the residuals were added to shapes predicted at maximum size values. This procedure ensures elimination of intraclade allometry while maintaining the interclade size-shape differences due to evolutionary allometry (Piras et al., 2011, 2014; Profico et al., 2017; Sansalone et al., 2018; Sansalone, Kotsakis, & Piras, 2015). This strategy, common in GMM studies, allows the standardization of shape variables at determined size values (Zelditch, Swiderski, & Sheets, 2012). The resulting data were used in all the following analyses.

Closely related species tend to be morphologically more similar to each other than to more distantly related taxa (Felsenstein, 1985). Therefore, the specimens cannot be treated as independent units of information (Garland & Ives, 2000). We used the K_{mult} statistic (Adams, 2014), a multivariate extension of Blomberg's K (Blomberg, Garland, & Ives, 2003), and the associated *p*-values, obtained via permutations of the data among the tree tips, to provide a metric of the strength of the phylogenetic signal on the shape of MB, LB, and face.

We assessed the covariation between MB and face, and LB and face using phylogenetically informed partial least squares (PLS) analyses (Bookstein, 1991; Rohlf & Corti, 2000). PLS is suitable for the study of covariation between two sets of variables in several groups (Bastir et al., 2010; McNulty, 2009; Neaux et al., 2018; Singh et al., 2012). Phylogenetically informed PLS estimates the degree of morphological covariation while accounting for phylogeny (Adams & Felice, 2014). This phylogenetic version of the PLS, suitable for highly multidimensional data, was implemented in the function phylo.integration() from the R package "geomorph" (Adams, Collyer, & Kaliontzopoulou, 2018). We quantified the covariation for each pair of axes by a correlation coefficient, which is supported by a permutation test for the null hypothesis that the distribution of specimens on one axis has no bearing on the distribution on the other axis. These methods are based on the analysis of the covariance structure of the different matrices corresponding to each identified modules. Additionally, we assessed the overall modularity between MB and face, and LB and face using the covariance ratio (CR). The value of CR provides a measure for characterizing and evaluating the degree of modularity in biological data sets (Adams, 2016; Adams & Collyer, 2016). This coefficient is a ratio of the overall covariation between modules relative to the overall covariation within modules. It is insensitive to sample size, number of variables, and display higher statistical power as compared to the frequently used RV coefficient (Escoufier, 1973; Klingenberg, 2009). The CR coefficient is computed on covariance matrices. We computed CR accounting for phylogenetic history using the function phylo.modularity() from "geomorph" (Adams et al., 2018). The CR coefficient for the observed modular hypothesis is compared to a distribution of values obtained by randomly assigning landmarks into subsets. A significant modular signal is found when the observed CR coefficient is small relative to this distribution (Adams, 2016). Such a result implies that there is significantly greater independence among modules than is expected under the null hypothesis of random associations of variables. This result is consistent with the identification of significant modular structure in the data. Values of CR lower than one suggest a strong degree of independence between the two structures. Values of CR greater than one indicate more integration between than within the studied structures, reflecting the absence of a modular structure.

We tested the relationship between ECV and MB, LB, and face structures, respectively, using a phylogenetic generalized least squares (PGLS) linear model (Adams & Collyer, 2016; Rohlf, 2001; Zelditch et al., 2012) using the function procD.pgls() from "geomorph"

TABLE 2 Definitions of midline basicranium (1–7), lateral basicranium (8–14), and face (15–29) landmarks

	Landmark	Definition
1	Foramen caecum	Most anterior inferior midline point of anterior cranial base
2	Posterior cribriform	Midline point at the posterior end of the cribriform plate
3	Sphenoidale	Most superior and posterior midline point on the jugum sphenoidale
4	Tuberculum sellae	Most superior and posterior midline point on the tuberculum sellae
5	Sella	Midline point at the center of the sella turcica
6	Posterior dorsum sellae	Midline point of the suture between the sphenoid and the basilar part of the occipital
7	Basion	Most anterior and inferior midline point on the margin of the foramen magnum
8	Anterior frontal	Most anterior point of the inner surface of the frontal bone, in the depression formed by the frontal pole
9	Posterior frontal	Point where the posterior border of the anterior fossa fuses with the endocranial lateral wall
10	Anterior clinoid process	Most superior, posterior, medial point of the anterior clinoid process
11	Petrous apex	Most superior, anterior, medial point of the margin of the apex of petrous part of the temporal bone
12	Foramen ovale	Most superior, posterior, lateral point of the margin of the foramen ovale
13	Internal accoustic meatus	Most inferior, anterior, medial point of the margin of the internal acoustic meatus
14	Pyramidal root	Point where the posterior pyramidal ridge meets the temporo-occipital suture
15	Glabella	Most anterior midline point on the frontal bone at the level of the supraorbital torus
16	Nasion	Midline intersection of nasal and frontal bones
17	Rhinion	Midline point at the inferior end of the internasal suture
18	Nasospinale	Most anterior midline point on nasal spine
19	Prosthion	Most anterior midline point of the maxillary alveolar process
20	Incisive canal	Point at the center of the incisive canal
21	Staphylion	Midline point on interpalatal suture corresponding to deepest point of notches at the rear of the palate
22	Superior margin of orbit	Most superior point of the superior margin of the orbit
23	Frontomalare orbitale	Point where the frontozygomatic suture crosses the inner orbital rim
24	Dacryon	Most superior point at which the lacrimomaxillary suture meets the frontal bone
25	Zygoorbitale	Point at which the zygomaticomaxillary suture meets the orbital rim
26	Zygomaxillare	Most inferior point of the zygomaticomaxillary suture
27	Alare	Most lateral point on the margin of the nasal aperture
28	Alveolar canine	Point in the center of the lateral border of the canine alveolus
29	Posterior alveolar	Most posterior point of the alveolar process on the inferior surface of the maxilla

(Adams et al., 2018) to account for the nonindependence among observations due to phylogenetic history. All analyses were performed on species averages.

3 | RESULTS

3.1 | Summary of the results

The morphological integration tests, using phylogenetically informed PLS, show highly significant integration degree between MB and face (r = .86; p < .01), and between LB and face (r = .91; p < .01) across primates. These results do not support the hypothesis that facial shape is significantly related to LB, but not to MB (hypothesis 1). Using PGLS regressions, we found a significant relationship between ECV and MB (PGLS-R^2; p < .01) but not between ECV and LB (PGLS-R^2 = 0.02; p = .16), in line with hypothesis 2.

3.2 | Evolutionary allometry

Multivariate regression of averaged per species shape coordinates against averaged per species logarithm of centroid size returned a significant result (F = 29.912; r^2 = .177; p < .01) indicating the relationship between shape and size is meaningful.

3.3 | Integration and modularity

The K_{mult} values indicate phylogenetic signal for MB (K_{mult} = 0.636, p < .01), LB (K_{mult} = 0.537, p < .01), and face (K_{mult} = 0.694, p < .01). The correlation coefficient of the first pair of phylogenetically informed PLS axes (PLS1) is strong and significant between MB and face (r = .86; p < .01; Figure 2). The PLS1 pair of axes account for 67.3% of the total covariance. For visualization purpose, we chose to defined triangular areas delimited by the landmarks used in the study

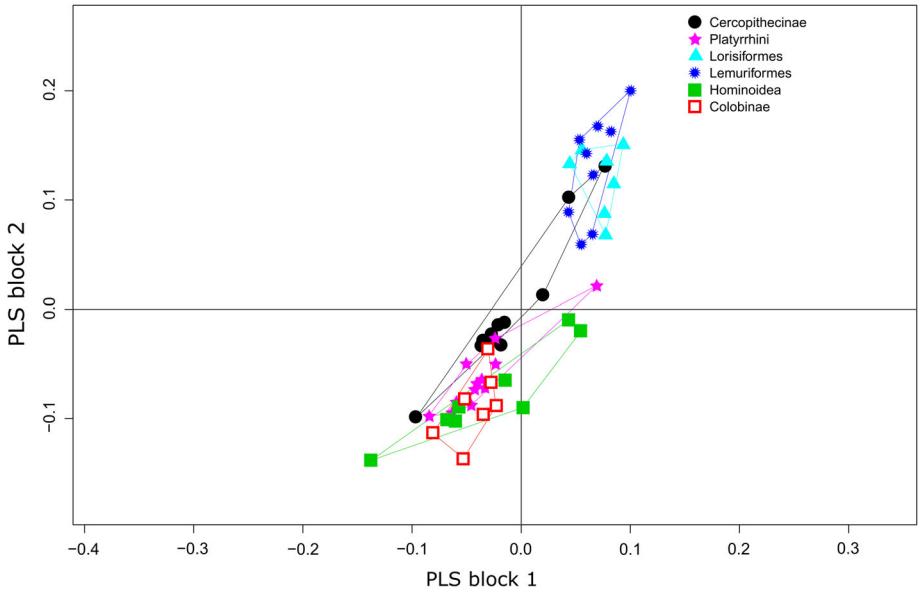

FIGURE 2 Scatter plot of the first partial least squares analysis axes between midline basicranium shape (block 1) and facial shape (block 2) depicting the significant integration relationship between these structures

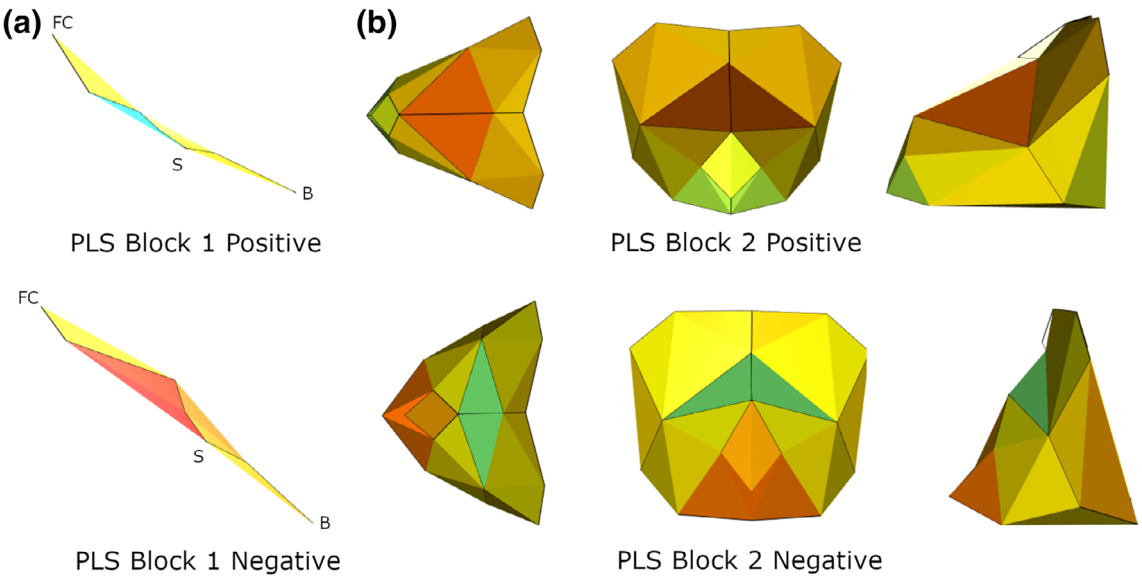

FIGURE 3 Wireframes showing shape changes along the singular axes of first pair of partial least squares analysis axes between the midline basicranium (a; block 1) and the face (b; block 2). Shape changes are depicted in lateral view for block 1 and in superior (far left), frontal (middle), and lateral (far right) views for block 2. Warmer colors indicate an increase in covariance in the surface area defined by the landmarks used in the study; colder colors indicate the opposite. Toward positive scores, a less flexed basicranium is associated with an anteroposteriorly longer face. B, Basion; Fc, Foramen caecum; S, Sella

(Figure 3). Warmer colors indicate an increase in the designated area surface. Toward positive scores, the basicranium is less flexed as the value of the angle formed by the posterior cribiform, sphenoidale, and basion angle increases (Figure 3). The midline region of the anterior cranial base (i.e., foramen caecum to sphenoidale) is shorter anteroposteriorly when compared to the middle and posterior cranial bases. Finally, the foramen magnum is displaced anteriorly and superiorly. These changes are associated with an anteroposteriorly longer face and palate. The upper face region (i.e., glabella, superior margin of the orbit, frontomalare orbitale, and dacryon) is larger while the lower face region (i.e., nasospinale, prosthion, alare, and alveolar canine) is narrower. The orbital frontation (i.e., the degree of verticality of the orbits) and orbital convergence (i.e., the degree to which the right and left orbits face in the same direction) is reduced (Ross, 1995). The correlation coefficient of PLS1 is also high and significant between LB and face ($r = .91$; $p < .01$; Figure 4) accounting for 86.4% of the total covariance. Toward positive scores the basicranium is anteroposteriorly shorter and mediolaterally narrower, especially in the middle cranial fossae (i.e., posterior frontal) and posterior cranial fossae (i.e., pyramidal root) regions (Figure 5). The face is superoinferiorly shorter and mediolaterally narrower, especially in the lower face region. The latter is also anteriorly projected relative to the upper face region.

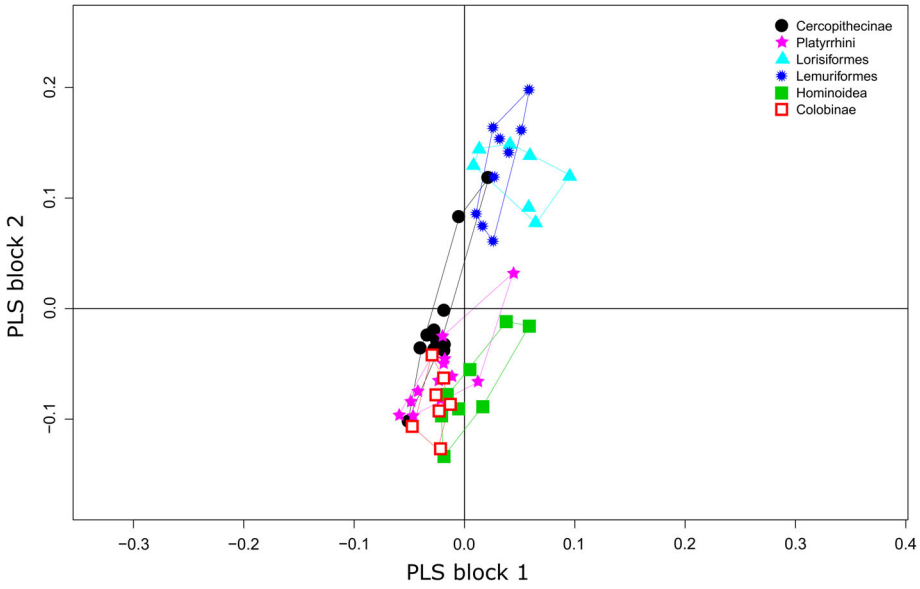

FIGURE 4 Scatter plot of the first partial least squares analysis axes between lateral basicranium shape (block 1) and facial shape (block 2) depicting the significant integration relationship between these structures

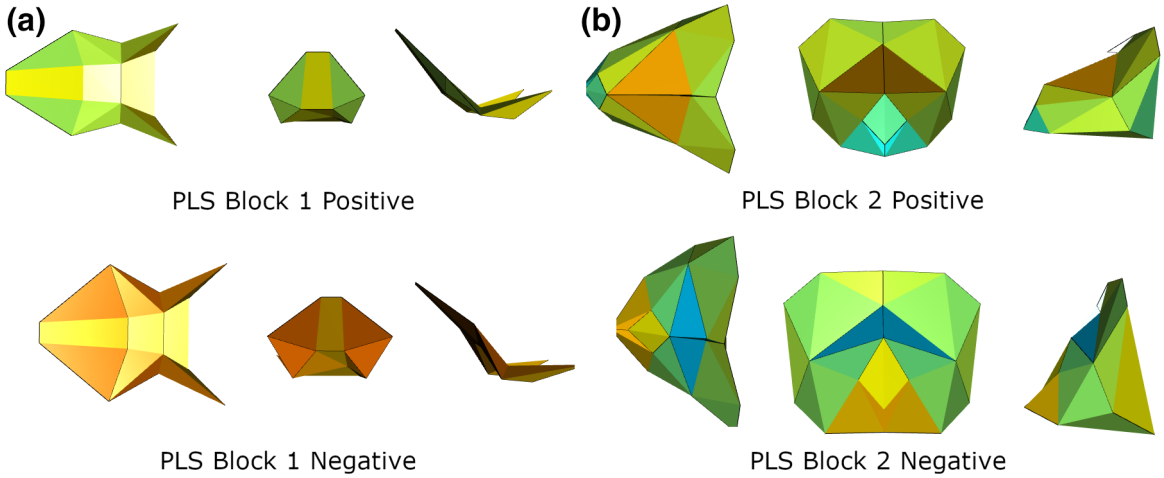

FIGURE 5 Wireframes showing shape changes along the singular axes of first pair of partial least squares analysis axes between the lateral basicranium (a; block 1) and the face (b; block 2). Shape changes are depicted in superior (far left), frontal (middle), and lateral (far right) views for block 1 and block 2. Warmer colors indicate an increase in covariance in the surface area defined by the landmarks used in the study; colder colors indicate the opposite. Toward positive scores, an anteroposteriorly shorter and mediolaterally narrower basicranium is associated with a superoinferiorly shorter, mediolaterally narrower, and anteriorly projected face

The size of the orbits and of the middle face region increases relative to the size of the face while the relative size of lower face region is reduced. Orbital frontation and convergence are reduced. Cardini (2018) recently proposed that splitting shape coordinates of landmarks into modules after a common superimposition, as it is done in our paper, can lead to spurious results. In this context, we decided to apply another method to our data (i.e., subdividing modules and performing separate Procrustes alignments; Klingenberg, 2011) to verify the presence of potentially ambiguous results. The tests return highly similar results when using the two different approaches (Appendix S3), suggesting that the degree of integration in our data is not influenced by the method chosen to generate shape coordinates for a priori defined modules. The covariance ratio values are greater than one, and *p*-values are not significant, indicating that there is more integration between than within the studied structures for MB and face (CR = 1.08; $p = .91$) and LB and face (CR = 1.03; $p = .07$) reflecting the absence of a modular structure. The PGLS regressions show a significant influence of ECV on the shape of MB (PGLS-$R^2 = 0.07$; $p < .01$) and face (PGLS-$R^2 = 0.05$; $p = .01$), meaning that ECV predicts respectively 7% and 5% of shape variation in these structures. The PGLS regression is not significant between ECV and LB (PGLS-$R^2 = 0.02$; $p = .16$).

4 | DISCUSSION

4.1 | Integration between craniofacial structures

Shape changes associated with the highly significant morphological integration between MB and face, and between LB and face across

primates correspond to the dolichocephalic and brachycephalic conditions that have been previously described in the primates (Neaux et al., 2018) and hominoids (Bastir & Rosas, 2004; Enlow & Hans, 1996; Mitteroecker & Bookstein, 2008; Neaux, 2017; Singh et al., 2012). Nonetheless, if the linear models computed in our work allow defining covariations between the studied structures, these models cannot accurately assess cause–effect relationships between these structures. The putative causal links proposed in the following discussion are therefore based on our current knowledge of the developmental and functional processes linking anatomical features. We found that covariation is stronger between, than within, the studied structures, reflecting the absence of a modular structure (Adams, 2016; Adams & Collyer, 2016). These results do not support hypothesis 1 as both LB and MB are significantly related to facial shape. In fact, the integration between MB and face is lower but still significant. Therefore, our results point to the presence of a pervasive integration between facial and basicranial structures (midline and lateral) in primates. At the order level, MB, LB, and face does not appear as separate modules but as integrated anatomical features belonging to the same global module. This strong correlation between craniofacial structures has been described previously in primates (Neaux et al., 2018), in hominoids (Neaux, 2017; Singh et al., 2012), and in platyrrhines (Makedonska, 2014; Marroig et al., 2004; Marroig & Cheverud, 2001). However, our findings contradict those of a recent study suggesting a greater independence between the face and the basicranium in hominoids and cercopithecines (Profico et al., 2017). If the anatomical landmarks selected to depict the face in this study are similar to ours, the basicranial landmark configuration is different as it describes only the shape of the occipital and temporal bones (Profico et al., 2017). This configuration composed of external landmarks located on the back of the cranial base therefore lack the shape information related the anterior and middle cranial fossae shape and relative orientation, both previously stated to be important in the relationship between face and cranial base (Bastir & Rosas, 2006, 2016; Gkantidis & Halazonetis, 2011; Neaux et al., 2013). These differences in landmark configuration may explain the significant independence between the face and the basicranium in this study (Profico et al., 2017). Our results therefore underline the importance of the definition of module boundaries in the interpretation of integration analyses (Goswami & Polly, 2010; Klingenberg, 2014). A corpus of studies based on anatomical network analyses (ANA), also found a greater modularity between facial and basicranial structures (Esteve-Altava, 2017; Esteve-Altava, Boughner, Diogo, Villmoare, & Rasskin-Gutman, 2015; Esteve-Altava, Marugán-Lobón, Botella, Bastir, & Rasskin-Gutman, 2013). This type of study differs from GMM approaches by defining modularity based on the topological relations (i.e., physical articulations) among bones in a predefined network model. The question of the comparison of modularity results obtained with GMM and ANA is still open as the nature of the correlation between shape and topology is still unclear (Esteve-Altava, 2017). More exploration of the relationship between the results obtained with these two methods (shape and topology) is therefore necessary to pinpoint the reasons of the differences in terms of modularity and integration between GMM and ANA studies.

Our results also highlight that the integration between LB and face and the relative independence of MB, previously described in hominids (Bastir & Rosas, 2005, 2006, 2009, 2016; Gkantidis & Halazonetis, 2011; Neaux et al., 2013), is not found among the other primate clades (cercopithecines, colobines, platyrrhines, lemuriformes, and lorisiformes) where we found a strong covariation between the craniofacial structures. Interestingly, Esteve-Altava et al. (2015) found that hominids display synapomorphies in the composition of their cranial modules (e.g., the presence of neurocranial and palatal modules) as well as large interspecific variations (e.g., the grouping of the frontal, sphenoid, and zygomatic bones in modules differs). In contrast, cercopithecids, platyrrhines, and strepsirrhines show minor intergroup differences. As explained above, these similarities should be treated with caution as the work of Esteve-Altava et al. (2015) considers a different definition of form (i.e., topology and arrangement and not size and shape), different component parts (individualized anatomical parts and not morphometric traits), and different relation among parts (topological boundaries and not covariations). Nonetheless, specificity of great apes regarding basicranial and facial module arrangement may explain the distinction between the "hominid integration type" observed previously (Bastir & Rosas, 2005, 2006, 2009, 2016; Gkantidis & Halazonetis, 2011; Neaux et al., 2013) and the "primate integration type" observed in the present study. The differences in integration level between our findings, in primates, and previous works, in hominids, may also be due to important differences in the variance structure. Our analyses, including a broad taxonomic sample, encompass a wider range of cranial shapes and therefore a greater magnitude of variance when compared to studies considering only humans and chimpanzees. This difference may explain why our work highlights correlations, such as the covariation between MB and face, which were not significant in previous studies (Bastir & Rosas, 2005, 2006, 2009, 2016; Gkantidis & Halazonetis, 2011; Neaux et al., 2013). The multiplication of integration studies at a high taxonomic scale (e.g., within primates) will allow a better assessment of the effect of intergroup variance in modularity analyses.

4.2 | Correlation of craniofacial structures with endocranial volume

Our results support the hypothesis that ECV is significantly related to MB (ECV predicts 7% of MB shape variation) but not to LB in primates (hypothesis 2). This result is in agreement with that of Aristide et al. (2015) who found a significant correlation between MB and ECV, but not between LB and ECV in platyrrhines. It also corroborates the hypothesis that changes in brain size play an important role specifically in MB shape changes (Bastir et al., 2010; Lieberman et al., 2000;Ross & Ravosa, 1993 ; Strait & Ross, 1999). As the relationship between LB and ECV is not significant, features other than brain size may affect the morphology of the lateral structures of the basicranium. Bastir, Rosas, Lieberman, and O'Higgins (2008) proposed that the shape of LB, and particularly of the middle cranial fossa housing the temporal lobes, is more related to brain shape rather than

brain size. Alternatively, LB morphology may be more related to variations in face and mandible morphology (Bastir & Rosas, 2006; Gkantidis & Halazonetis, 2011; Neaux et al., 2013), and projection (Bastir & Rosas, 2016). In particular, Bastir and Rosas (2016) show that in hominids, an anterior projection of LB, that is, a more anterior position of the sphenoid wings relative to the sphenoid body, is related to an anterior projection of facial structures, independent of MB.

Our results also further show a significant interaction between ECV and the face. This correlation is likely an indirect consequence of the integration between basicranial and facial structures. It has been hypothesized that brain size increase led to the midsagittal flexion of the cranial base, which caused a "mechanical" downward rotation of the face (Enlow & Azuma, 1975; McCarthy & Lieberman, 2001; Neaux, Gilissen, Coudyzer, & Guy, 2015). This "facial orientation hypothesis" states that the face is characterized by a structural unit, called the "facial block," composed of the frontal bones, the anterior cranial fossa, and the ethmomaxillary complex (i.e., the ethmoid bone, the maxillary bone, and the hard palate; McCarthy & Lieberman, 2001). It takes into account the fact that the angle between the anterior part of the cranial base (i.e., the anterior cranial fossae) and the posterior part of the face is constant, around 90° (Bromage, 1992; Enlow & Azuma, 1975; Enlow & Hans, 1996; McCarthy & Lieberman, 2001). Therefore, a downward rotation of the anterior cranial fossa, caused by an increase of brain size, may lead to a downward rotation of the entire facial block, explaining the relationship between ECV and face.

5 | CONCLUSIONS

Our results do not support hypothesis 1, that is, that facial shape is significantly related to LB but not to MB. Instead, we found a strong and pervasive integration in craniofacial structures across primates, in contrast to previous results in hominids (Bastir & Rosas, 2006; Gkantidis & Halazonetis, 2011; Neaux et al., 2013). The great variations and the uniqueness of module organization in great apes (Esteve-Altava et al., 2015) may explain this distinction between the "primate integration type" and the "hominid integration type." The important variance in our study due to its broad taxonomic sample may also be responsible for the overall integration in our findings. Our results are consistent with the hypothesis that ECV is significantly related to MB but not to LB in primates. This highlights the significant effect of brain size on the shape of the midline structures of the cranial base (Ross & Ravosa, 1993; Strait & Ross, 1999). The lateral basicranium is possibly more strongly influenced by brain shape rather than brain size (Bastir et al., 2008) and by variations in facial and mandibular shape and projection (Bastir & Rosas, 2016; Lieberman et al., 2000; Neaux et al., 2013).

The linear models used in this study have been sufficient to identify covariations between basicranium, face, and ECV, yet they cannot accurately assess cause–effect relationships between these features. Future studies should therefore focus on the definition of the causal links between these variables to define the processes involved in the setup of the great cranial morphological diversity of primates (Gonzalez-Voyer & von Hardenberg, 2014; von Hardenberg & Gonzalez-Voyer, 2013).

ACKNOWLEDGMENTS

We thank the Smithsonian's Division of Mammals (Dr. K. Helgen) and Human Origins Program (Dr. M. Tocheri) for the scans of the National Museum of Natural History specimens used in this research. These scans were acquired through the support of the Smithsonian 2.0 Fund and the Smithsonian's Collections Care and Preservation Fund. We also wish to thank the following institutions for allowing us the access to their specimens: the Museum of Comparative Zoology at Harvard University, the Natural History Museum, and the Duke Lemur Center. This work was supported by an Australian Research Council (ARC) Discovery grant (DP140102659) to S.W.

ORCID

Dimitri Neaux https://orcid.org/0000-0001-9465-220X

REFERENCES

Adams, D. C. (2014). A generalized K statistic for estimating phylogenetic signal from shape and other high-dimensional multivariate data. *Systematic Biology*, *63*(5), 685–697.

Adams, D. C. (2016). Evaluating modularity in morphometric data: Challenges with the RV coefficient and a new test measure. *Methods in Ecology and Evolution*, *7*(5), 565–572.

Adams, D. C., Collyer, M., & Kaliontzopoulou, A. (2018). geomorph: Geometric Morphometric Analyses of 2D/3D Landmark Data (Version 3.0.7).

Adams, D. C., & Collyer, M. L. (2016). On the comparison of the strength of morphological integration across morphometric datasets. *Evolution*, *70*(11), 2623–2631.

Adams, D. C., & Felice, R. N. (2014). Assessing trait covariation and morphological integration on phylogenies using evolutionary covariance matrices. *PLoS One*, *9*(4), e94335.

Aguilar, M., Boyer, D., Carney, C., Gonzales, L., Griffin, R., Griffith, D., … Schaeffer, M. (2017). Gonzales skull project. *MorphoSource*.

Aguilar, M., Boyer, D., Heritage, S., Kay, R., Riddle, C., & Seiffert, E. (2017). Duke lemur center, division of fossil primates. *MorphoSource*.

Allen, K., & Schaeffer, M. (2017). Allen primate skull collection. *MorphoSource*.

Aristide, L., dos Reis, S. F., Machado, A. C., Lima, I., Lopes, R. T., & Perez, S. I. (2015). Encephalization and diversification of the cranial base in platyrrhine primates. *Journal of Human Evolution*, *81*, 29–40.

Arnold, C., Matthews, L. J., & Nunn, C. L. (2010). The 10kTrees website: A new online resource for primate phylogeny. *Evolutionary Anthropology*, *19*, 114–118.

Bastir, M., & Rosas, A. (2004). Facial heights: Evolutionary relevance of postnatal ontogeny for facial orientation and skull morphology in humans and chimpanzees. *Journal of Human Evolution*, *47*(5), 359–381.

Bastir, M., & Rosas, A. (2005). Hierarchical nature of morphological integration and modularity in the human posterior face. *American Journal of Physical Anthropology*, *128*(1), 26–34.

Bastir, M., & Rosas, A. (2006). Correlated variation between the lateral basicranium and the face: A geometric morphometric study in different human groups. *Archives of Oral Biology*, *51*(9), 814–824.

Bastir, M., & Rosas, A. (2009). Mosaic evolution of the basicranium in *Homo* and its relation to modular development. *Evolutionary Biology*, *36*(1), 57–70.

Bastir, M., & Rosas, A. (2016). Cranial base topology and basic trends in the facial evolution of Homo. *Journal of Human Evolution*, *91*, 26–35.

Bastir, M., Rosas, A., Lieberman, D. E., & O'Higgins, P. (2008). Middle cranial fossa anatomy and the origin of modern humans. *The Anatomical Record*, *291*(2), 130–140.

Bastir, M., Rosas, A., & O'Higgins, P. (2006). Craniofacial levels and the morphological maturation of the human skull. *Journal of Anatomy*, *209* (5), 637–654.

Bastir, M., Rosas, A., Stringer, C., Cuétara, J. M., Kruszynski, R., Weber, G. W., … Ravosa, M. J. (2010). Effects of brain and facial size on basicranial form in human and primate evolution. *Journal of Human Evolution*, *58*(5), 424–431.

Bennett, C. V., & Goswami, A. (2012). Morphometric analysis of cranial shape in fossil and recent euprimates. *Anatomy Research International*, *2012*, e478903.

Blomberg, S. P., Garland, T., & Ives, A. R. (2003). Testing for phylogenetic signal in comparative data: Behavioral traits are more labile. *Evolution; International Journal of Organic Evolution*, *57*(4), 717–745.

Bookstein, F. L. (1991). *Morphometric tools for landmark data: Geometry and biology*. Cambridge, England: Cambridge University Press.

Bromage, T. G. (1992). The ontogeny of *Pan troglodytes* craniofacial architectural relationships and implications for early hominids. *Journal of Human Evolution*, *23*(3), 235–251.

Cardini, A. (2018). Integration and modularity in Procrustes shape data: Is there a risk of spurious results? *Evolutionary Biology*, *46*(1), 90–105.

Cardini, A., Seetah, K., & Barker, G. (2015). How many specimens do I need? Sampling error in geometric morphometrics: Testing the sensitivity of means and variances in simple randomized selection experiments. *Zoomorphology*, *134*(2), 149–163.

Copes, L., Kaufman, S., & Lee, J. G. (2017). Lucas & Copes MCZ scans. *MorphoSource*.

Enlow, D. H., & Azuma, M. (1975). Functional growth boundaries in the human and mammalian face. In D. Bergsma (Ed.), *Morphogenesis and malformation of face and brain* (pp. 217–230). New York, NY: Alan R. Liss.

Enlow, D. H., & Hans, M. G. (1996). *Essentials of facial growth*. Philadelphia, PA: Saunders.

Escoufier, Y. (1973). Le traitement des variables vectorielles. *Biometrics*, *29*, 751–760.

Esteve-Altava, B. (2017). Challenges in identifying and interpreting organizational modules in morphology. *Journal of Morphology*, *278*, 960–974.

Esteve-Altava, B., Boughner, J. C., Diogo, R., Villmoare, B. A., & Rasskin-Gutman, D. (2015). Anatomical network analysis shows decoupling of modular lability and complexity in the evolution of the primate skull. *PLoS One*, *10*(5), e0127653.

Esteve-Altava, B., Marugán-Lobón, J., Botella, H., Bastir, M., & Rasskin-Gutman, D. (2013). Grist for Riedl's mill: A network model perspective on the integration and modularity of the human skull. *Journal of Experimental Zoology Part B: Molecular and Developmental Evolution*, *320*(8), 489–500.

Felsenstein, J. (1985). Confidence limits on phylogenies: An approach using the bootstrap. *Evolution*, *39*(4), 783–791.

Fleagle, J. G., Gilbert, C. C., & Baden, A. L. (2010). Primate cranial diversity. *American Journal of Physical Anthropology*, *142*(4), 565–578.

Fleagle, J. G., Gilbert, C. C., & Baden, A. L. (2016). Comparing primate crania: The importance of fossils. *American Journal of Physical Anthropology*, *161*(2), 259–275.

Garland, T., & Ives, A. R. (2000). Using the past to predict the present: Confidence intervals for regression equations in phylogenetic comparative methods. *The American Naturalist*, *155*(3), 346–364.

Gkantidis, N., & Halazonetis, D. J. (2011). Morphological integration between the cranial base and the face in children and adults. *Journal of Anatomy*, *218*(4), 426–438.

Gonzalez-Voyer, A., & von Hardenberg, A. (2014). An introduction to phylogenetic path analysis. In L. Z. Garamszegi (Ed.), *Modern phylogenetic comparative methods and their application in evolutionnary biology* (pp. 201–209). Heidelberg, Germany: Springer.

Goswami, A., & Polly, P. D. (2010). Methods for studying morphological integration and modularity. *The Paleontological Society Papers*, *16*, 213–243.

Goswami, A., & Polly, P. D. (2014). The macroevolutionary consequences of phenotypic integration: From development to deep time. *Philosophical Transactions of the Royal Society of London. Series B, Biological Sciences*, *369*(1649), 20130254.

Groves, C. P. (2001). *Primate taxonomy*. Washington, DC: Smithsonian Institution.

Klingenberg, C. P. (2005). Developmental constraints, modules, and evolvability. In B. Hallgrímsson & B. K. Hall (Eds.), *Variation: A central concept in biology* (pp. 1–30). Amsterdam, Netherlands: Elsevier Academic Press.

Klingenberg, C. P. (2008). Morphological integration and developmental modularity. *Annual Review of Ecology, Evolution, and Systematics*, *39*, 115–132.

Klingenberg, C. P. (2009). Morphometric integration and modularity in configurations of landmarks: Tools for evaluating a priori hypotheses. *Evolution & Development*, *11*(4), 405–421.

Klingenberg, C. P. (2010). Evolution and development of shape: Integrating quantitative approaches. *Nature Reviews Genetics*, *11*(9), 623–635.

Klingenberg, C. P. (2011). MorphoJ: An integrated software package for geometric morphometrics. *Molecular Ecology Resources*, *11*(2), 353–357.

Klingenberg, C. P. (2014). Studying morphological integration and modularity at multiple levels: Concepts and analysis. *Philosophical Transactions of the Royal Society of London. Series B, Biological Sciences*, *369* (1649), 20130249.

Klingenberg, C. P., Barluenga, M., & Meyer, A. (2002). Shape analysis of symmetric structures: Quantifying variation among individuals and asymmetry. *Evolution; International Journal of Organic Evolution*, *56*(10), 1909–1920.

Klingenberg, C. P., & Marugán-Lobón, J. (2013). Evolutionary covariation in geometric morphometric data: Analyzing integration, modularity, and allometry in a phylogenetic context. *Systematic Biology*, *62*(4), 591–610.

Lieberman, D. E. (2011). *The evolution of the human head*. Cambridge, MA: Harvard University Press.

Lieberman, D. E., & McCarthy, R. C. (1999). The ontogeny of cranial base angulation in humans and chimpanzees and its implications for reconstructing pharyngeal dimensions. *Journal of Human Evolution*, *36* (5), 487–517.

Lieberman, D. E., Ross, C. F., & Ravosa, M. J. (2000). The primate cranial base: Ontogeny, function, and integration. *American Journal of Physical Anthropology*, *Suppl. 31*, 117–169.

Makedonska, J. (2014). New insights into the phenotypic covariance structure of the anthropoid cranium. *Journal of Anatomy*, *225*(6), 634–658.

Marcucio, R. S., Young, N. M., Hu, D., & Hallgrimsson, B. (2011). Mechanisms that underlie co-variation of the brain and face. *Genesis*, *49*(4), 177–189.

Marroig, G., & Cheverud, J. M. (2001). A comparison of phenotypic variation and covariation patterns and the role of phylogeny, ecology, and ontogeny during cranial evolution of new world monkeys. *Evolution; International Journal of Organic Evolution*, *55*(12), 2576–2600.

Marroig, G., De Vivo, M., & Cheverud, J. M. (2004). Cranial evolution in sakis (Pithecia, Platyrrhini). II: Evolutionary processes and morphological integration. *Journal of Evolutionary Biology*, *17*(1), 144–155.

Martínez-Abadías, N., Esparza, M., Sjøvold, T., & Hallgrímsson, B. (2016). Chondrocranial growth, developmental integration and evolvability in the human skull. In J. C. Boughner & C. Rolian (Eds.), *Developmental approaches to human evolution* (pp. 17–34). Hoboken, NJ: John Wiley & Sons.

McCarthy, R. C., & Lieberman, D. E. (2001). Posterior maxillary (PM) plane and anterior cranial architecture in primates. *The Anatomical Record*, *264*(3), 247–260.

McNulty, K. P. (2009). Computing singular warps from Procrustes aligned coordinates. *Journal of Human Evolution*, *57*(2), 191–194.

Mittermeier, R. A., Rylands, A. B., & Wilson, D. E. (2013). *Handbook of the mammals of the world, Vol. 3: Primates*. Barcelona, Spain: Lynx Edicions.

Mitteroecker, P., & Bookstein, F. (2007). The conceptual and statistical relationship between modularity and morphological integration. *Systematic Biology*, *56*(5), 818–836.

Mitteroecker, P., & Bookstein, F. (2008). The evolutionary role of modularity and integration in the hominoid cranium. *Evolution*, *62*(4), 943–958.

Neaux, D. (2017). Morphological integration of the cranium in *Homo*, *Pan*, and *Hylobates* and the evolution of hominoid facial structures. *American Journal of Physical Anthropology*, *162*(4), 732–746.

Neaux, D., Gilissen, E., Coudyzer, W., & Guy, F. (2015). Implications of the relationship between basicranial flexion and facial orientation for the evolution of hominid craniofacial structures. *International Journal of Primatology*, *36*(6), 1120–1131.

Neaux, D., Guy, F., Gilissen, E., Coudyzer, W., & Ducrocq, S. (2013). Covariation between midline cranial base, lateral basicranium, and face in modern humans and chimpanzees: A 3D geometric morphometric analysis. *The Anatomical Record*, *296*(4), 568–579.

Neaux, D., Sansalone, G., Ledogar, J. A., Heins Ledogar, S., Luk, T. H. Y., & Wroe, S. (2018). Basicranium and face: Assessing the impact of morphological integration on primate evolution. *Journal of Human Evolution*, *118*, 43–55.

Parsons, T. E., Downey, C. M., Jirik, F. R., Hallgrimsson, B., & Jamniczky, H. A. (2015). Mind the gap: Genetic manipulation of basicranial growth within synchondroses modulates calvarial and facial shape in mice through epigenetic interactions. *PLoS One*, *10*(2), e0118355.

Parsons, T. E., Schmidt, E. J., Boughner, J. C., Jamniczky, H. A., Marcucio, R. S., & Hallgrímsson, B. (2011). Epigenetic integration of the developing brain and face. *Developmental Dynamics*, *240*(10), 2233–2244.

Piras, P., Buscalioni, A. D., Teresi, L., Raia, P., Sansalone, G., Kotsakis, T., & Cubo, J. (2014). Morphological integration and functional modularity in the crocodilian skull. *Integrative Zoology*, *9*(4), 498–516.

Piras, P., Salvi, D., Ferrara, G., Maiorino, L., Delfino, M., Pedde, L., & Kotsakis, T. (2011). The role of post-natal ontogeny in the evolution of phenotypic diversity in *Podarcis* lizards. *Journal of Evolutionary Biology*, *24*(12), 2705–2720.

Profico, A., Piras, P., Buzi, C., Di Vincenzo, F., Lattarini, F., Melchionna, M., … Manzi, G. (2017). The evolution of cranial base and face in Cercopithecoidea and Hominoidea: Modularity and morphological integration. *American Journal of Primatology*, *79*(12), e22721.

R Core Team. (2017). R: A language and environment for statistical computing. Vienna, Austria.

Ritzman, T. B., Banovich, N., Buss, K. P., Guida, J., Rubel, M. A., Pinney, J., … Stone, A. C. (2017). Facing the facts: The Runx2 gene is associated with variation in facial morphology in primates. *Journal of Human Evolution*, *111*, 139–151.

Rohlf, F. J. (2001). Comparative methods for the analysis of continuous variables: Geometric interpretations. *Evolution; International Journal of Organic Evolution*, *55*(11), 2143–2160.

Rohlf, F. J., & Corti, M. (2000). Use of two-block partial least-squares to study covariation in shape. *Systematic Biology*, *49*(4), 740–753.

Rohlf, F. J., & Slice, D. (1990). Extensions of the Procrustes method for the optimal superimposition of landmarks. *Systematic Biology*, *39*(1), 40–59.

Ross, C. F., & Ravosa, M. J. (1993). Basicranial flexion, relative brain size, and facial kyphosis in nonhuman primates. *American Journal of Physical Anthropology*, *91*(3), 305–324.

Ross, C. F. (1995). Allometric and functional influences on primate orbit orientation and the origins of the Anthropoidea. *Journal of Human Evolution*, *29*(3):201–227.

Rylands, A. B., & Mittermeier, R. A. (2014). Primate taxonomy: Species and conservation. *Evolutionary Anthropology*, *23*, 8–10.

Sansalone, G., Colangelo, P., Kotsakis, T., Loy, A., Castiglia, R., Bannikova, A. A., … Piras, P. (2018). Influence of evolutionary allometry on rates of morphological evolution and disparity in strictly subterranean moles (Talpinae, Talpidae, Lipotyphla, Mammalia). *Journal of Mammalian Evolution*, *25*(1), 1–14.

Sansalone, G., Kotsakis, T., & Piras, P. (2015). *Talpa fossilis* or *Talpa europaea*? Using geometric morphometrics and allometric trajectories of humeral moles remains from Hungary to answer a taxonomic debate. *Palaeontologia Electronica*, *18*(2), 1–17.

Schlager, S., & Jefferis, G. (2016). Morpho: Calculations and visualisations related to geometric morphometrics (Version 2.4.1.1).

Schlosser, G., & Wagner, G. P. (2004). *Modularity in development and evolution*. Chicago, IL: University of Chicago Press.

Schroeder, L., & von Cramon-Taubadel, N. (2017). The evolution of hominoid cranial diversity: A quantitative genetic approach. *Evolution*, *71*(11), 2634–2649.

Singh, N., Harvati, K., Hublin, J.-J., & Klingenberg, C. P. (2012). Morphological evolution through integration: A quantitative study of cranial integration in *Homo*, *Pan*, *Gorilla* and *Pongo*. *Journal of Human Evolution*, *62*(1), 155–164.

Strait, D. S. (2001). Integration, phylogeny, and the hominid cranial base. *American Journal of Physical Anthropology*, *114*, 273–297.

Strait, D. S., & Ross, C. F. (1999). Kinematic data on primate head and neck posture: Implications for the evolution of basicranial flexion and an evaluation of registration planes used in paleoanthropology. *American Journal of Physical Anthropology*, *108*(2), 205–222.

von Hardenberg, A., & Gonzalez-Voyer, A. (2013). Disentangling evolutionary cause-effect relationships with phylogenetic confirmatory path analysis. *Evolution*, *67*(2), 378–387.

Wagner, G. P., & Altenberg, L. (1996). Perspective: Complex adaptations and the evolution of evolvability. *Evolution; International Journal of Organic Evolution*, *50*(3), 967–976.

Wagner, G. P., Pavlicev, M., & Cheverud, J. M. (2007). The road to modularity. *Nature Reviews. Genetics*, *8*(12), 921–931.

Wiley, D., Amenta, N., Alcantara, D., Ghosh, D., Kil, Y. J., Delson, E., … O'Neill, R. (2005). *Evolutionary morphing*. Proceedings of IEEE visualization 2005, Minneapolis, MN, 431–438.

Zelditch, M. L., Swiderski, D. L., & Sheets, H. D. (2012). *Geometric morphometrics for biologists: A primer* (2nd ed.). San Diego, CA: Academic Press.

SUPPORTING INFORMATION

Additional supporting information may be found online in the Supporting Information section at the end of this article.

How to cite this article: Neaux D, Wroe S, Ledogar JA, Heins Ledogar S, Sansalone G. Morphological integration affects the evolution of midline cranial base, lateral basicranium, and face across primates. *Am J Phys Anthropol*. 2019;1–11. https://doi.org/10.1002/ajpa.23899